Separation and Purification Technology 323 (2023) 124390

Contents lists available at ScienceDirect

Separation and Purification Technology

journal homepage: www.elsevier.com/locate/seppur

Customized hourglass-shaped channels in a copper(II)-organic framework for one-step ethylene purification from ethylene/ethane/acetylene ternary mixtures with high adsorption capacity

Lu-Lu Ma [a,b], Jiaqi Liu [b], Qian Xu [a], Hao Wang [b,*], Guo-Ping Yang [a,*], Yao-Yu Wang [a,*]

[a] Key Laboratory of Synthetic and Natural Functional Molecule Chemistry of the Ministry of Education, Shaanxi Key Laboratory of Physico-Inorganic Chemistry, College of Chemistry & Materials Science, Northwest University, Xi'an 710127, PR China
[b] Hoffmann Institute of Advanced Materials, Shenzhen Polytechnic, 7098 Liuxian Blvd., Nanshan, Shenzhen 518055, Guangdong, PR China

ARTICLE INFO

Keywords:
Metal–organic frameworks
C2 hydrocarbon
Selective adsorption
Multicomponent separation

ABSTRACT

One-step purification of C_2H_4 from $C_2H_2/C_2H_4/C_2H_6$ ternary mixtures represents an important yet challenging task in chemical industry. Favored adsorption of C_2H_2 and C_2H_6 over C_2H_4 has stringent requirements on pore size and surface chemistry of the adsorbents. We report a Cu-MOF (**Cu–L**), $[Cu_{0.5}(L)_{0.5}]\cdot 2DMF$ (H_2L = 4′-(1H-1,2,4-triazol-1-yl)-[1,1'-biphenyl]-3,5-dicarboxyl)) with one-dimensional hourglass-shaped channels decorated by phenyl rings and triazole units. Suitable pore structure and customized pore surface have endowed **Cu–L** with high adsorption capacities toward C_2 hydrocarbons, and preferential adsorption of C_2H_2 and C_2H_6 over C_2H_4. Separation capability of **Cu–L** has been confirmed by multicomponent breakthrough experiments and polymer-grade C_2H_4 can be directly obtained from $C_2H_2/C_2H_6/C_2H_4$ (1/1/1 and 1/9/90, v/v/v) mixtures. The underlying mechanism of preferential adsorption was revealed by Grand Canonical Monte Carlo simulations and DFT calculations.

1. Introduction

As an essential raw material for a variety of organic products, ethylene (C_2H_4) is of paramount importance in petrochemical industry [1–3]. The main method for C_2H_4 production in industry is steam or thermal cracking of either naphtha or ethane (C_2H_6). Crude product of cracking is usually accompanied by C_2H_2 and C_2H_6 as impurities [4–6]. Due to the similar molecular size and boiling points of C_2H_2, C_2H_4 and C_2H_6, the subsequent separation process is very challenging (Table S1) [7,8]. At present, C_2H_2 is removed by solvent extraction or catalytic hydrogenation, followed by cryogenic distillations for the separation of C_2H_6 and C_2H_4 [9–11]. The process is not only technically complicated, but also energy-intensive. Therefore, developing simpler and more energy-efficient technologies such as adsorptive separation for one-step purification of C_2H_4 from $C_2H_2/C_2H_4/C_2H_6$ mixtures is crucial and imparative [12,13].

Various porous materials have been investigated for adsorptive separation of C_2 hydrocarbons [14–16]. In particular, metal–organic frameworks (MOFs) showed great promise in separating C_2 binary mixtures such as C_2H_2/C_2H_4, C_2H_6/C_2H_4 and C_2H_2/CO_2 because of their structural diversity, highly tunable pore size and surface chemistry [17,18]. However, one-step purification of C_2H_4 from $C_2H_2/C_2H_4/C_2H_6$ ternary mixtures through preferential adsorption of C_2H_2 and C_2H_6 over C_2H_4 remains a daunting challenge. This is because the quadrupole moment and kinetic diameter of C_2H_4 (1.5×10^{-26} esu cm^2 and 4.1 Å) lie between those of C_2H_2 (7.2×10^{-26} esu cm^2 and 3.3 Å) and C_2H_6 (0.65×10^{-26} esu cm^2 and 4.4 Å). A couple of MOFs that show preferential adsorption of C_2H_6 and C_2H_2 over C_2H_4 have been reported over the past few years [19–21]. These studies demonstrated that pore surface chemistry control is the key to achieving one-step C_2H_4 purification. In general, nonpolar pore surface may be favorable to the adsorption of C_2H_6 but not to C_2H_2. Thus, it is important to find the the "sweet spot" by creating optimal chemical environment on the pore surface and suitable pore dimensions so as to achieve simultaneously preferred adsorption for both C_2H_2/C_2H_4 and C_2H_6/C_2H_4.

Herein, we report a Cu-MOF, $[Cu_{0.5}(L)_{0.5}]\cdot 2DMF$ (**Cu–L**) (H_2L = 4′-(1H-1,2,4-triazol-1-yl)-[1,1'-biphenyl]-3,5-dicarboxyl), where its hourglass-shaped channels were decorated by a high density of phenyl/triazole groups. The compound exhibited high adsorption capacities for C_2H_2 and C_2H_6, with uptake of 125.3 and 109.1 cm^3 g^{-1}, respectively at

* Corresponding authors.
E-mail addresses: wanghao@szpt.edu.cn (H. Wang), ygp@nwu.edu.cn (G.-P. Yang), wyaoyu@nwu.edu.cn (Y.-Y. Wang).

https://doi.org/10.1016/j.seppur.2023.124390
Received 11 May 2023; Received in revised form 18 June 2023; Accepted 19 June 2023
Available online 22 June 2023

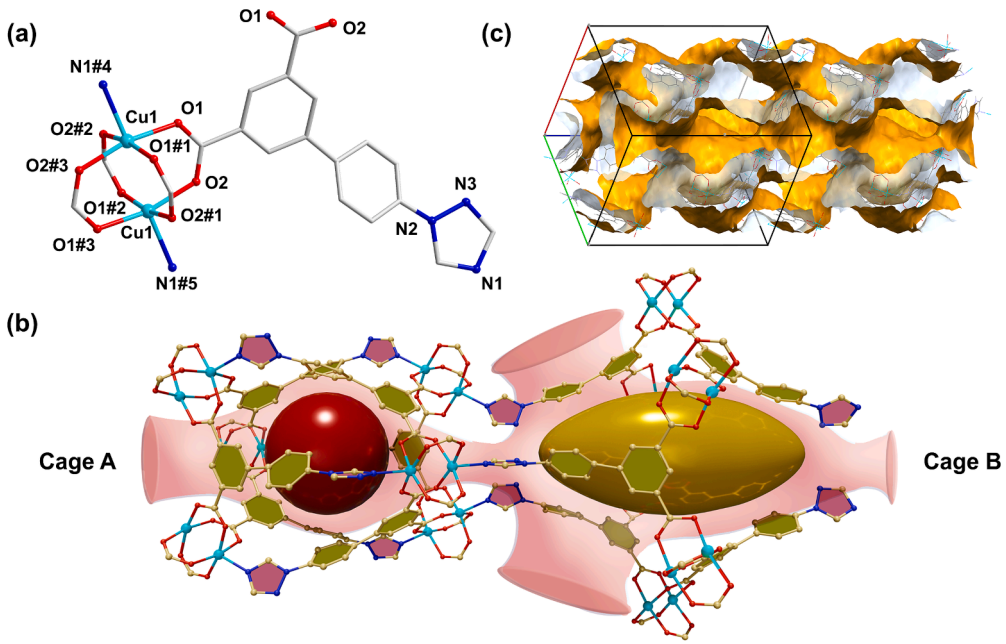

Fig. 1. (a) Coordination environment of Cu^{2+} ions in **Cu–L** (Cu: cyan, C: gray, N: blue, O: red) (Symmetry codes: #1 = 1 − x, 1 − y, z; #2 = x, y, 1 − z; #3 = 1 − x, 1 − y, 1 − z; #4 = 2/3 + x − y, 4/3 − y, z − 1/3; #5 = 1/3 − x + y, y − 1/3, 4/3 − z); (b) Cage A and cage B form hourglass-shaped channel along with side open window in **Cu–L**; (c) 1D channel viewed along the c axis (yellow: inner surface of pores; gray: outer surface of pores).

298 K and 100 kPa. The values are higher than that for C_2H_4 under identical conditions, leading to an adsorption selectivity of 1.6 for both C_2H_2/C_2H_4 and C_2H_6/C_2H_4. The high adsorption capacity and simultaneously favored adsorption of C_2H_2 and C_2H_6 over C_2H_4 render **Cu–L** the capability for one-step C_2H_4 purification from $C_2H_2/C_2H_4/C_2H_6$ ternary mixtures. Its separation capability has been confirmed by multicomponent breakthrough tests where polymer-grade C_2H_4 was directly obtained. The underlying mechanism of preferential adsorption by **Cu–L** was uncovered by DFT calculations and Grand Canonical Monte Carlo simulations, demonstrating the key role of the phenyl rings in selective trapping C_2H_6 and C_2H_2.

2. Materials and characterization

2.1. Materials and general methods

All chemicals for synthesis were purchased commercially without further purification. Elemental analyses of C, H, and N were determined with a Perkin-Elmer 2400C elemental analyzer. Thermogravimetric analyses (TGA) were carried out in a nitrogen stream using a Netzsch TG209F3 equipment at a heating rate of 10 °C min^{-1}. Single crystal X-ray diffraction data were collected on a Bruker SMART APEX II CCD single crystal diffractometer. Gas adsorption measurements were performed with an automatic volumetric sorption apparatus (Micrometrics ASAP 2020 M). Breakthrough tests were carried out by an auto mixed-gas breakthrough apparatus (3P MIXSORB) equipped with vapor generator.

2.2. Synthesis of $[Cu_{0.5}(L)_{0.5}]$·2DMF

A glass vial (10 mL) containing H_2L (4.3 mg, 0.0014 mmol), $Cu(NO_3)_2{\cdot}3H_2O$ (3.4 mg, 0.014 mmol), DMF (1.5 mL), HNO_3 (65%, 40 μL) was heated at 95 °C for 16 h, and then cooled to room temperature. Green hexagonal block-shaped crystals were isolated in 63% yield. Anal. Calcd. for $C_{16}H_9CuN_3O_4$: C, 51.75; H, 2.42; N, 11.32%. Found: C, 51.12; H, 2.65; N, 11.61%. FT-IR data (KBr, cm^{-1}): 3423(w), 3118(m), 2929 (m), 1664(s), 1529(m), 1369(s), 1282(w), 1145(w), 1095(w), 975(w), 842(w), 775(s), 732(m), 673(w).

2.3. X-ray crystallography

Single crystal X-ray diffraction data of compound **Cu–L** were collected at 150.0 K on a Bruker SMART APEX II CCD detector using Mo radiation (λ = 0.71073 Å). The structure was solved by direct methods and refined on F^2 by full matrix least-squares methods. The non-H atoms were refined anisotropically, while the H atoms fixed to their geometrically ideal positions were refined isotropically. It was failed to refine the solvent molecules in **Cu–L**, thereby the SQUEEZE routine of PLATON program was used in structural refinement. Relevant crystallographic results were listed in Table S2. The refinement results and selected bond distances/angles were given in Table S3.

2.4. Adsorption isotherms

Before gas adsorption experiments, all the as-synthesized samples were activated under vacuum at 473 K for 12 h. Gas adsorption measurements were carried out using Micrometrics ASAP 2020 M and TriStar 3020 gas adsorption analyzers.

3. Results and discussion

3.1. Structural analysis

Single-crystal X-ray diffraction showed that **Cu–L** crystallizes in the trigonal crystal system with *R*-3 m space group (CCDC No.: 2173089). The asymmetric unit contains a half of Cu^{2+} ion and a half of L^{2-} ligand (Fig. 1a). The structure is built on commonly observed $[Cu_2(COO)_4]$ paddle wheel secondary building units (SBUs) where two Cu^{2+} are coordinated by four carboxylate bridges and the SBUs were further connected through triazole portion of the organic linker. The final structure features honeycomb 3D network with 1D hourglass channels (Fig. 1b), and the channel interiors were decorated with abundant phenyl/triazole rings and uncoordinated nitrogen atoms. Hourglass channels provide favorable conditions for gas storage, and the channels decorated with abundant phenyl/triazole rings and uncoordinated nitrogen atoms lay the foundation for gas separation. The overall framework of **Cu–L** can be simplified as a (3, 6)-c **eea** net (Figure S2). As seen from Fig. 1c, the

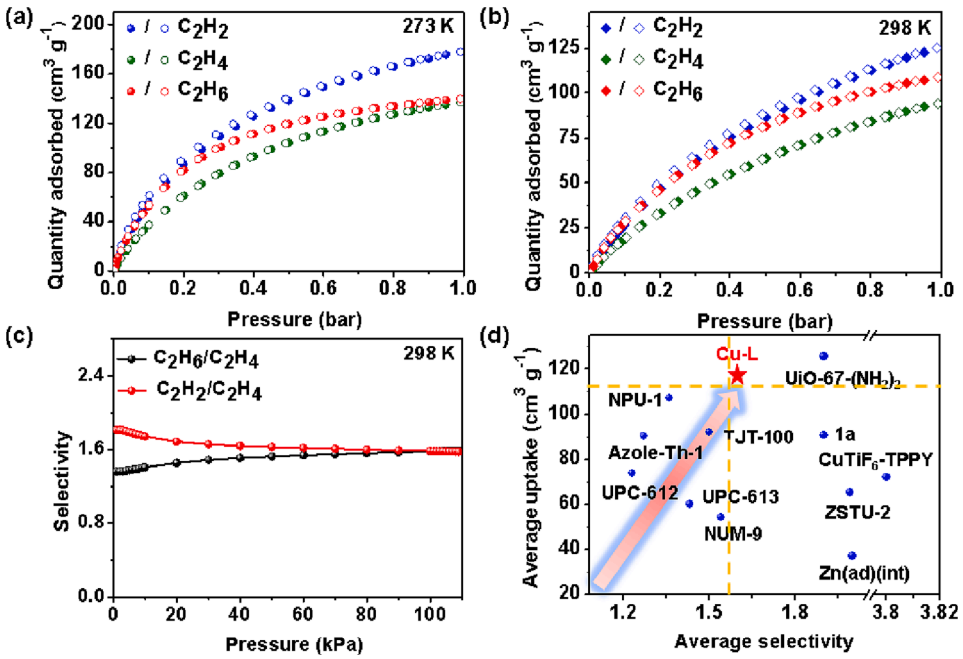

Fig. 2. C_2H_6, C_2H_4 and C_2H_2 sorption isotherms at 273 K (a) and 298 K (b); (c) IAST selectivity of **Cu–L** for equimolar C_2H_2/C_2H_4 and C_2H_6/C_2H_4 binary mixtures at 298 K; (d) comparison of average uptake (C_2H_2 and C_2H_6) and selectivity (C_2H_2/C_2H_4 and C_2H_6/C_2H_4) for reported MOFs explored for C_2 separation.

hourglass channels of **Cu–L** consist of two type cages. The spherical cage is ~9 Å in diameter, and the elliptic cage is about 9 Å × 22 Å. PLATON calculation revealed a total accessible volume of 49.5% for **Cu–L** upon guest removal.

3.2. Material stability

The PXRD pattern of the as-synthesized sample of **Cu–L** matched well with the theoretical one, confirming the phase purity of the compound (Figure S3). Thermogravimetric analysis (TGA) curve of the as-synthesized **Cu–L** showed a weight loss of 43.7% before 270 °C which should be correlated to the loss of guest solvent DMF (Figure S5). The compound can be fully activated by heating at 200℃ for 12 h under high vacuum. **Cu–L** retained its crystallinity upon thermal activation or being treated with various organic solvents (Figure S3 and S4).

3.3. Gas adsorption and separation

Permanent porosity of **Cu–L** was evaluated by N_2 adsorption at 77 K. The adsorption displayed a typical Type-I profile with a saturated adsorption capacity of 409.5 $cm^3\ g^{-1}$ (Figure S7a). Langmuir and Brunauer-Emmett-Teller (BET) surface areas were calculated to be 1707 and 1160 $m^2\ g^{-1}$, respectively. According to the Horvath-Kawazoe (H-K) model, the pore size distribution of **Cu–L** centered at 8.8–10.0 Å, consistent with the values measured from its crystal structure.

Single-component adsorption isotherms of C_2H_2, C_2H_4, and C_2H_6 in **Cu–L** were collected at both 273 and 298 K. The compound displayed reversible Type I adsorption profiles for all three gases, and the adsorption capacities at 1 bar and 273 K are 177.9, 137.1 and 139.9 $cm^3\ g^{-1}$ for C_2H_2, C_2H_4 and C_2H_6, respectively (Fig. 2a). The uptake values decrease slightly to 125.3, 94.6 and 109.1 $cm^3\ g^{-1}$ for C_2H_2, C_2H_4 and C_2H_6, respectively, at 298 K (Fig. 2b). These results suggest **Cu–L** shows favored adsorption of C_2H_2 and C_2H_6 over C_2H_4. Notably, its adsorption capacities toward C_2 hydrocarbons are among the highest for reported adsorbents explored for C_2 separations. We compared the average uptake of C_2H_2 and C_2H_6 at 298 K and 100 kPa for reported MOFs and the results are shown in Fig. 2d. The value for **Cu–L** (117.2 $cm^3\ g^{-1}$) is slightly lower than that of UiO-67-$(NH_2)_2$ (125.6 $cm^3\ g^{-1}$)[12] under the same conditions but exceeds all other materials including Azoe-Th-1 (90.5 cm3 g^{-1}), [22] NPU-1 (107.4 $cm^3\ g^{-1}$), [23] 1a (90.7 $cm^3\ g^{-1}$), [24] TJT-100 (91.9 $cm^3\ g^{-1}$), [25] UPC-612 (73.6 $cm^3\ g^{-1}$), [26] UPC-613 (54.3 $cm^3\ g^{-1}$), [26] Zn(ad)(int) (37.2 $cm^3\ g^{-1}$) [19].

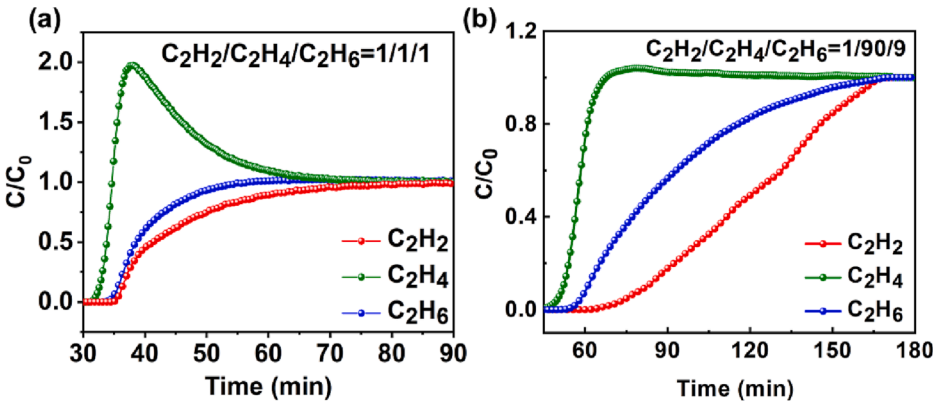

Fig. 3. The dynamic breakthrough curves of **Cu–L** for $C_2H_2/C_2H_4/C_2H_6$ (1/1/1, v/v/v) (a) and $C_2H_2/C_2H_4/C_2H_6$ (1/90/9, v/v/v) (b) mixtures at 298 K.

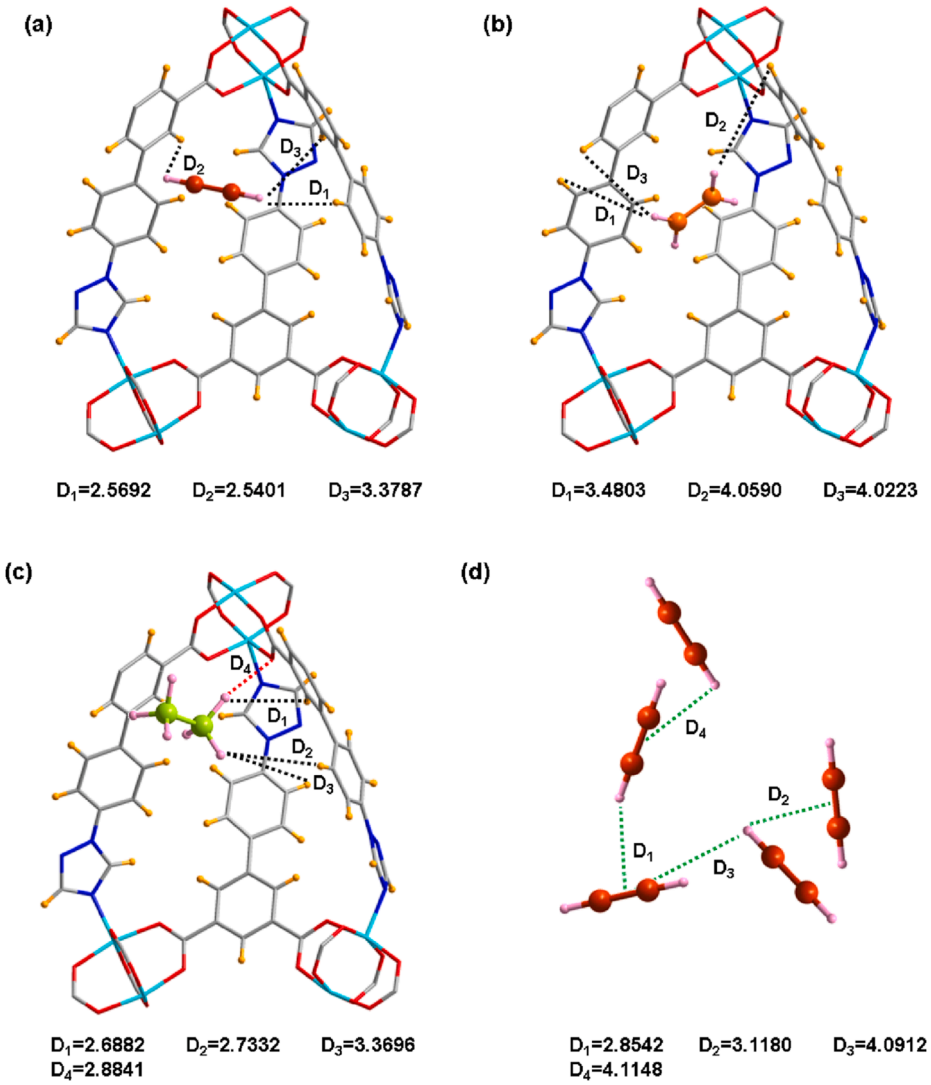

Fig. 4. Preferential binding sites of C_2 molecules in **Cu–L** for C_2H_2 (a), C_2H_4 (b) and C_2H_6 (c); (d) packing of C_2H_2 molecules in the channels of Cu–L, distances are in Å. (Cu: cyan, C: gray/dark red/organge/green, N: blue, O: red, H: gold/pink).

In order to quantitatively evaluate the interactions between the skeleton and gas molecules, isosteric heats of adsorption (Q_{st}) of C_2H_6, C_2H_4 and C_2H_2 were calculated using Virial equation. The initial Q_{st} value for **Cu–L** follows the sequence of: $Q_{st}(C_2H_2)$ (30.0 kJ mol^{-1}) > $Q_{st}(C_2H_6)$ (28.4 kJ mol^{-1}) > $Q_{st}(C_2H_4)$ (23.1 kJ mol^{-1}) (Figure S8a), which is consistent with their gas adsorption tendency at low pressure, confirming that **Cu–L** showed preferential adsorption toward C_2H_2 and C_2H_6 over C_2H_4. In addition, compared with the values for $Fe_2(O_2)$(dobdc) (67 kJ mol^{-1}), [27] IRMOF-8 (52.5 kJ mol^{-1}) [28] and UTSA-60a (36 kJ mol^{-1}), [29] lower $Q_{st}(C_2H_6)$ of **Cu–L** indicated that lower energy consumption for adsorbent regeneration.

Adsorption selectivities of **Cu–L** for C_2H_6/C_2H_4 and C_2H_2/C_2H_4 mixtures were calculated by applying ideal adsorbed solution theory (IAST). As shown in Fig. 2c, **Cu–L** shows an adsorption selectivity of 1.6 for both C_2H_2/C_2H_4 and C_2H_2/C_2H_4 at 298 K and 1 bar. The value is comparable to most of the reported adsorbents tested for C_2 ternary separations [22,23,30]. It is important for an adsorbent to possess high adsorption capacities and balanced adsorption selectivities for the separation of $C_2H_4/C_2H_2/C_2H_6$ ternary mixtures and thus **Cu–L** holds great promise for this separation.

3.4. Breakthrough experiment

Multicomponent column breakthrough tests were carried out to verify the separation capability of **Cu–L** for C_2 ternary mixtures. The separation of two different compositions of $C_2H_2/C_2H_4/C_2H_6$ (1/1/1, v/v/v) and $C_2H_2/C_2H_4/C_2H_6$ (1/90/9, v/v/v) mixtures were evaluated. As shown in Fig. 3a, for a ternary mixture of $C_2H_2/C_2H_4/C_2H_6$ (1/1/1, v/v/v), C_2H_4 eluted out first at the 30th minute, while C_2H_2 and C_2H_6 were retained in the column for a longer time, breaking through at the 33rd and 34th minute. The dynamic adsorption capacity of **Cu–L** was calculated to be 46.07 cm^3 g^{-1}, 34.49 cm^3 g^{-1}, 40.55 cm^3 g^{-1} for C_2H_2, C_2H_4, and C_2H_6, respectively. Dynamic adsorption capacities were slightly lower than that of static adsorption, which may be caused by the competitive adsorption sites of the three gases at the same time. The results confirmed that **Cu–L** can separate $C_2H_2/C_2H_4/C_2H_6$ ternary mixtures and produce polymer grade (99.95+%) C_2H_4 directly. Separation experiment for a more industrially relevant mixture of $C_2H_2/C_2H_4/C_2H_6$ (1/90/9, v/v/v) was subsequently performed (Fig. 3b). Again, C_2H_4 broke out first at the 37th minute, followed by C_2H_6 at 51st minute and C_2H_2 at the 62nd minute. Polymer grade (99.95+%) C_2H_4 with a productivity of 1.07 L kg^{-1} was directly obtained through a single breakthrough test. In addition, the crystallinity of **Cu–L** remains intact after the breakthrough experiment, indicating its highly robust

framework (Figure S3).

3.5. Molecular simulations

To further explore the underlying mechanism of selective adsorption by **Cu–L**, Grand Canonical Monte Carlo (GCMC) simulation was carried out to investigate the interaction between the skeleton and C_2 gas molecules. Calculations showed that C_2 gas molecules in **Cu–L** interact with multiple sites. Figure S11 showed that the density distribution of C_2H_6, C_2H_4 and C_2H_2 after three gas components were introduced into the structure and adsorption equilibrium was reached. The adsorption zone was located at the middle of the cage cavity, near the phenyl groups of the organic linker. In general, the distances between C_2H_6/C_2H_2 and the framework were notably shorter than that of C_2H_4, suggesting stronger van der Waals forces of the former two gases with the framework (Fig. 4a-4c). This is consistent with the calculated heats of adsorption and the sequence of adsorption capacities. In particular, besides the strong van der Waals force generated by the interaction between C_2H_2 and phenyl groups in **Cu–L**, the interaction between adjacent adsorbed C_2H_2 molecules also showed strong $C\text{-}H_{C2H2}\cdot\cdot\ \pi_{C2H2}$ contact ($H\cdot\cdot\pi = 2.8542–4.1148$ Å), facilitating C_2H_2 accumulation in the cage cavity (Fig. 4d). This unique interaction between C_2H_2 molecules may be responsible for the higher absorption capacity of C_2H_2 relative to C_2H_4 and C_2H_6. In contrast, strong interaction between adsorbed adjacent C_2H_6 were not observed. The calculated binding energies are C_2H_2 (34.78 kJ mol^{-1}) > C_2H_6 (31.48 kJ mol^{-1}) > C_2H_4 (30.05 kJ mol^{-1}), which is consistent with the aforementioned results.

4. Conclusions

In summary, we report a Cu-MOF (**Cu–L**) with hourglass channels showing high adsorption capacities and balanced adsorption selectivity for $C_2H_2/C_2H_4/C_2H_6$ separation. Single component adsorption and multicomponent breakthrough experiments demonstrated that **Cu–L** can simultaneously remove C_2H_2 and C_2H_6 from the ternary C_2 mixtures to generate polymer-grade C_2H_4 by one step. Molecular simulation studies showed that the selective adsorption of **Cu–L** should be attributed to the phenyl groups decorating its channels. Our study may shed light on design strategies for further development of MOFs with tailored pore structure for C_2 hydrocarbon separations.

CRediT authorship contribution statement

Lu-Lu Ma: Investigation, Writing – original draft. **Jiaqi Liu:** Investigation, Data curation. **Qian Xu:** Visualization. **Hao Wang:** Supervision, Writing – original draft. **Guo-Ping Yang:** Conceptualization, Supervision. **Yao-Yu Wang:** Conceptualization, Funding acquisition.

Declaration of Competing Interest

The authors declare the following financial interests/personal relationships which may be considered as potential competing interests: [Guo-Ping Yang reports financial support was provided by National Natural Science Foundation of China. Hao Wang reports financial support was provided by Shenzhen Science and Technology Innovation Committee.].

Data availability

Data will be made available on request.

Acknowledgements

This work is financially supported by by the National Natural Science Foundation of China (22071194, and 21971207) and Shenzhen Science and Technology Program (RCYX20200714114539243).

Appendix A. Supplementary material

Supplementary data to this article can be found online at https://doi.org/10.1016/j.seppur.2023.124390.

References

[1] D.S. Sholl, R.P. Lively, Seven chemical separations to change the world, Nature 532 (2016) 435.
[2] S. Chu, Y.i. Cui, N. Liu, The path towards sustainable energy, Nat. Mater. 16 (1) (2017) 16–22.
[3] L. Zhang, L. Li, E. Hu, L. Yang, K. Shao, L. Yao, K. Jiang, Y. Cui, Y. Yang, B. Li, B. Chen, G. Qian, Boosting ethylene/ethane separation within copper(I)-chelated metal-organic frameworks through tailor-made aperture and specific π-complexation, Adv. Sci. 7 (2020) 1901918.
[4] J.-R. Li, R.J. Kuppler, H.-C. Zhou, Selective gas adsorption and separation in metal–organic frameworks, Chem. Soc. Rev. 38 (2009) 1477–1504.
[5] J.-W. Cao, S. Mukherjee, T. Pham, Y. Wang, T. Wang, T. Zhang, X. Jiang, H.-J. Tang, K.A. Forrest, B. Space, M.J. Zaworotko, K.-J. Chen, One-step ethylene production from a four-component gas mixture by a single physisorbent, Nat. Commun. 12 (2021) 6507.
[6] S. Geng, E.n. Lin, X. Li, W. Liu, T. Wang, Z. Wang, D. Sensharma, S. Darwish, Y. H. Andaloussi, T. Pham, P. Cheng, M.J. Zaworotko, Y. Chen, Z. Zhang, Scalable room-temperature synthesis of highly robust ethane-selective metal-organic frameworks for efficient ethylene purification, J. Am. Chem. Soc. 143 (23) (2021) 8654–8660.
[7] J. Liu, J. Miao, H. Wang, Y. Gai, J. Li, Enhanced one-step purification of C2H4 from C2H2/C2H4/C2H6 mixtures by fluorinated Zr-MOF, AIChE J. (2023) e18021.
[8] P. Liu, Y. Wang, Y. Chen, J. Yang, X. Wang, L. Li, J. Li, Construction of saturated coordination titanium-based metal–organic framework for one-step $C_2H_2/C_2H_6/C_2H_4$ separation, Sep. Purif. Technol. 276 (2021), 119284.
[9] K.-J. Chen, D.G. Madden, S. Mukherjee, T. Pham, K.A. Forrest, A. Kumar, B. Space, J. Kong, Q.-Y. Zhang, M.J. Zaworotko, Synergistic sorbent separation for one-step ethylene purification from a four-component mixture, Science 366 (6462) (2019) 241–246.
[10] T. Ren, M. Patel, K. Blok, Olefins from conventional and heavy feedstocks: Energy use in steam cracking and alternative processes, Energy 31 (2006) 425–451.
[11] S. Laha, N. Dwarkanath, A. Sharma, S. Balasubramanian, T.K. Maji, Tailoring a robust Al-MOF for trapping C_2H_6 and C_2H_2 towards efficient C_2H_4 purification from quaternary mixtures, Chem. Sci. 13 (2022) 7172.
[12] X.-W. Gu, J.-X. Wang, E. Wu, H. Wu, W. Zhou, G. Qian, B. Chen, B. Li, Immobilization of Lewis basic sites into a stable ethane-selective MOF enabling one-step separation of ethylene from a ternary mixture, J. Am. Chem. Soc. 144 (6) (2022) 2614–2623.
[13] Z. Belohlav, P. Zamostny, T. Herink, The kinetic model of thermal cracking for olefins production, Chem. Eng. Process 42 (6) (2003) 461–473.
[14] W. Wang, L. Wang, F. Du, G.-D. Wang, L. Hou, Z. Zhu, B.o. Liu, Y.-Y. Wang, Dative B←N bonds based crystalline organic framework with permanent porosity for acetylene storage and separation, Chem. Sci. 14 (3) (2023) 533–539.
[15] P.-Q. Liao, W.-X. Zhang, J.-P. Zhang, X.-M. Chen, Efficient purification of ethene by an ethane-trapping metal-organic framework, Nat. Commun. 6 (2015) 8697.
[16] G. Narin, V.F.D. Martins, M. Campo, A.M. Ribeiro, A. Ferreira, J.C. Santos, K. Schumann, A.E. Rodrigues, Light olefins/paraffins separation with 13X zeolite binderless beads, Sep. Purif. Technol. 133 (2014) 452–475.
[17] P.J. Bereciartua, Á. Cantín, A. Corma, J.L. Jordá, M. Palomino, F. Rey, S. Valencia, E.W. Corcoran, P. Kortunov, P.I. Ravikovitch, A. Burton, C. Yoon, Y.u. Wang, C. Paur, J. Guzman, A.R. Bishop, G.L. Casty, Control of zeolite framework flexibility and pore topology for separation of ethane and ethylene, Science 358 (6366) (2017) 1068–1071.
[18] Q. Liu, S.G. Cho, J. Hilliard, T.Y. Wang, S.C. Chien, L.C. Lin, A.C. Co, C.R. Wade, Inverse CO_2/C_2H_2 separation with MFU-4 and selectivity reversal via postsynthetic ligand exchange, Angew. Chem. Int. Ed. 63 (2023) e202218854.
[19] Q. Ding, Z. Zhang, Y. Liu, K. Chai, R. Krishna, S. Zhang, One-step ethylene purification from ternary mixtures in a metal-organic framework with customized pore chemistry and shape, Angew. Chem. Int. Ed. 61 (2022) e202208134.
[20] P. Zhang, Y. Zhong, Y. Zhang, Z. Zhu, Y. Liu, Y. Su, J. Chen, S. Chen, Z. Zeng, H. Xing, S. Deng, J. Wang, Synergistic binding sites in a hybrid ultramicroporous material for one-step ethylene purification from ternary C2 hydrocarbon mixtures, Sci. Adv. 8 (2022) eabn9231.
[21] Y. Wang, M. Fu, S. Zhou, H. Liu, X. Wang, W. Fan, Z. Liu, Z. Wang, D. Li, H. Hao, X. Lu, S. Hu, D. Sun, Guest-molecule-induced self-adaptive pore engineering facilitates purification of ethylene from ternary mixture, Chem 8 (12) (2022) 3263–3274.
[22] Z. Xu, X. Xiong, J. Xiong, R. Krishna, L. Li, Y. Fan, F. Luo, B. Chen, A robust Th-azole framework for highly efficient purification of C_2H_4 from a $C_2H_4/C_2H_2/C_2H_6$ mixture, Nat. Commun. 11 (2020) 3163–3172.
[23] B. Zhu, J.-W. Cao, S. Mukherjee, T. Pham, T. Zhang, T. Wang, X. Jiang, K. A. Forrest, M.J. Zaworotko, K.-J. Chen, Pore engineering for one-step ethylene purification from a three-component hydrocarbon mixture, J. Am. Chem. Soc. 143 (3) (2021) 1485–1492.
[24] G.-D. Wang, Y.-Z. Li, W.-J. Shi, L. Hou, Y.-Y. Wang, Z. Zhu, One-step C_2H_4 purification from ternary $C_2H_6/C_2H_4/C_2H_2$ mixtures by a robust metal-organic framework with customized pore environment, Angew. Chem. Int. Ed. 134 (2022) e202205427.

[25] H.-G. Hao, Y.-F. Zhao, D.-M. Chen, J.-M. Yu, K. Tan, S. Ma, Y. Chabal, Z.-M. Zhang, J.-M. Dou, Z.-H. Xiao, G. Day, H.-C. Zhou, T.-B. Lu, Simultaneous trapping of C_2H_2 and C_2H_6 from a ternary mixture of $C_2H_2/C_2H_4/C_2H_6$ in a robust metal-organic framework for the purification of C_2H_4, Angew. Chem. Int. Ed. 57 (49) (2018) 16067–16071.

[26] Y. Wang, C. Hao, W. Fan, M. Fu, X. Wang, Z. Wang, L. Zhu, Y. Li, X. Lu, F. Dai, Z. Kang, R. Wang, W. Guo, S. Hu, D. Sun, One-step ethylene purification from an acetylene/ethylene/ethane ternary mixture by cyclopentadiene cobalt-functionalized metal-organic frameworks, Angew. Chem. Int. Ed. 60 (20) (2021) 11350–11358.

[27] L. Li, R.-B. Lin, R. Krishna, H. Li, S. Xiang, H. Wu, J. Li, W. Zhou, B. Chen, Ethane/ethylene separation in a metal-organic framework with iron-peroxo sites, Science 362 (6413) (2018) 443–446.

[28] J. Pires, M.L. Pinto, V.K. Saini, Ethane selective IRMOF-8 and Its significance in ethane-ethylene separation by adsorption, ACS Appl. Mater. Interfaces 6 (15) (2014) 12093–12099.

[29] H.-M. Wen, B. Li, H. Wang, C. Wu, K. Alfooty, R. Krishna, B. Chen, A microporous metal–organic framework with rare *lvt* topology for highly selective C_2H_2/C_2H_4 separation at room temperature, Chem. Commun. 51 (26) (2015) 5610–5613.

[30] S.-Q. Yang, F.-Z. Sun, P. Liu, L. Li, R. Krishna, Y.-H. Zhang, Q. Li, L. Zhou, T.-L. Hu, Efficient purification of ethylene from C_2 hydrocarbons with an C_2H_6/C_2H_2-selective metal-organic framework, ACS Appl. Mater. Interfaces 13 (1) (2021) 962–969.